Lasers in Manufacturing Conference 2019

Additive Manufacturing of CuSn10 Powder via Selective Laser Melting

N. Emminghaus[a]*, C. Hoff[a], J. Hermsdorf[a], S. Kaierle[a]

[a]*Laser Zentrum Hannover e. V., Hollerithallee 8, D-30419 Hannover, Germany*

Abstract

Selective laser melting offers the possibility of manufacturing parts with complex geometries and a wide range of materials. Besides steel, aluminum or titanium alloys for which the process has been studied extensively, copper alloys are of great importance especially due to their unique physical properties. Facing difficulties such as high thermal conductivity, low absorption and resulting poor reproducibility, there is still a great need to optimize the manufacturing process and to describe the influence of the process parameters on the component quality.
In this study the influence of laser power, scanning speed and hatch distance as well as interactions of these parameters on the mechanical properties and the relative density were investigated for the bronze CuSn10 using an industrial plant (Yb-fiberlaser, power: 250 W, beam diameter: 40 µm). The parameters are configured according to Design of Experiments enabling an efficient and economical way of evaluating the occurring effects.

Keywords: Selective laser melting; additive manufacturing; copper alloy; mechanical properties

1. Introduction

The selective laser melting, also known as laser powder bed fusion (LPBF), is an additive manufacturing technique. Parts are built layer by layer using metal powder that is molten in every layer according to sliced 3D CAD models. Advantages of this manufacturing technique include the producibility of complex geometries, like lightweight structures and internal cooling systems and that no additional tools are required. LPBF processed parts also provide different microstructures and therefore different mechanical properties compared to conventionally fabricated parts due to rapid cooling.

* Corresponding author. Tel.: +49 511 2788-355; fax: +49051102788-100.
E-mail address: n.emminghaus@lzh.de.

A wide range of materials (mainly iron-, titanium- and nickel-based alloys) has been processed successfully via laser powder bed fusion (Jia and Gu, 2014; Sun et al., 2016; Zhang and Attar, 2015). Now the additive manufacturing of copper and copper alloys attracts growing attention (Frigola et al., 2008; Ramirez et al.,2011) attributed to their unique physical properties like high wear and corrosion resistance as well as high electrical and thermal conductivity. Related to these properties, there is a wide field of important industrial applications, for example bearings, marine parts, pump housings, gears and heat exchangers (Mao et al., 2017; Scudino et al., 2015; Barik et al., 2005).

The main difficulties in processing copper and copper alloys via LPBF are the low laser absorption and the high thermal conductivity, which is desirable for the use in thermal management systems but leads to aggravation of the melting process (Mao et al., 2017; Liu et al., 2014). Consequently, higher laser power and scanning speed compared with other materials are required to fabricate dense parts (Becker et al., 2009, Becker, 2010). On the other side most industrial plants are only equipped with lasers providing a maximum power of 200 W, which is not sufficient for pure copper (Meiners, 2011).

An additional difficulty relating to the processing of copper and bronze powders is that due to the high ductility the powder particles tend to agglomerate. Thereby the flowability and post-process powder removal are impaired (Frigola et al., 2014).

To achieve optimal process stability and parts with maximum relative density, the optimal processing parameters have to be found and correlations between them and the resulting part quality need to be identified. Different research works were carried out for copper and bronze and the maximum relative density achieved was 99.97 % for the copper alloy Cu-10Zn (Zhang et al., 2019). The goal of achieving a 100 % relative density could not be reached yet. In none of the studies a DOE approach was used to evaluate parameter effects and interactions.

Therefore, the aim of this work is to find the optimal processing parameters for the bronze CuSn10 and to identify effects and interactions between them by applying statistical methods of the Design of Experiments.

2. Material and Methods

2.1. Experimental Materials

The material used for building the specimens was gas-atomized CuSn10 powder produced by TLS Technik GmbH & Co. Spezialpulver KG with a particle size of 10 - 45 µm. A particle size analysis conducted by TLS Technik showed that 10 % of the particles have a diameter smaller than 10.46 µm and 90 % smaller than 47.32 %. The chemical analysis revealed that the actual value of the tin content is 10.10 %. To evaluate the particle geometry SEM (scanning electron microscopy) images, shown in Fig. 1, were taken and analyzed. As the images show, the powder consisted of mostly spherical particles.

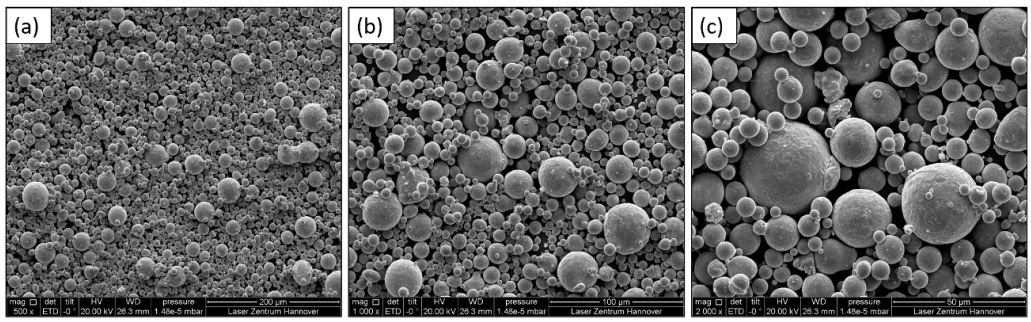

Fig. 1. SEM images of CuSn10 powder: (a) magnification x500; (b) magnification x1000; (c) magnification x2000

2.2. Experimental Equipment

For the implementation of the experiments, the industrial plant Orlas Creator (O.R. Lasertechnologie GmbH, Dieburg, Germany) was used. The laser source is a continuous wave ytterbium fiber single mode laser operating at a wavelength of 1070 nm with a maximum power of 250 W providing a laser beam with a M^2 factor of 1.05, which quantifies the beam quality. The plant is equipped with a galvanoscanner and an f-Theta lens. It offers a minimum beam diameter of 40 µm and building volume of Ø 100 mm x 100 mm. The process chamber is filled by the inert gas argon to avoid oxidation, realizing a minimum residual oxygen content of 0.1-0.15 %.

2.3. Experimental Methods

The experimental investigations were carried out on cubic specimens with a side length of 5 mm. A constant layer thickness of 25 µm, a beam diameter of 40 µm and an powder feed rate of 220 % were adjusted and the oxygen level was kept at the minimum between 0.1 and 0.15 %. A cross-hatching scanning strategy (zigzag) was employed with a rotation angle of 45 ° between adjacent layers, pictured in Fig. 2. The varied factors whose influence is analyzed in the investigations are the factors that generally have the greatest influence on the processing results according to literature and former experiments with other materials:

- Laser power (LP)
- Scanning speed (SS)
- Hatch distance (HD)

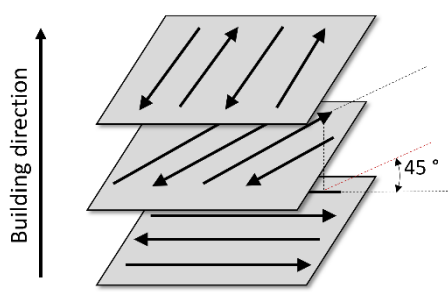

Fig. 2. Cross-hatching scanning strategy [modified from Mao et al., 2017]

The processing parameters were varied according to Design of Experiments (DoE). Two experimental runs were conducted. In the first run a total amount of 43 specimens were processed, which was the maximum number of specimens possible to process in one build job. This run was meant to give a first overview of relatively optimal parameter settings. The experimental design contained two center points to detect non-linear effects. Based on the manufacturers recommendations for the settings for processing of the bronze powder as well as the settings found in the literature, the upper and lower limits for the parameter variation were chosen. Varying them in 5 stages made it possible to detect linear, quadratic and cubic effects and up to third degree interactions between the parameters. In the second run, 33 specimens, three of them center points, were built and the limits of the parameter values were set based on the results of the first run to take a closer look on the supposedly optimal parameters. To reduce the evaluation effort, the number of specimens was reduced by 10 in this run. The different values of the processing parameters in the two experimental runs can be overviewed in Table 1. The experimental designs for both runs were constructed with the help of the statistics software JMP (SAS Institute GmbH, Böblingen, Germany). To find the optimal design for the chosen limits and number of specimens, the Custom Design option was used.

Table 1. Values of processing parameters

Processing parameter	Values in first run	Values in second run
Laser power	100 / 125 / 150 / 175 / 200 W	140 / 160 / 180 / 200 / 220 W
Scanning speed	600 / 800 / 1000 / 1200 / 1400 mm/s	600 / 800 / 1000 / 1200 / 1400 mm/s
Hatch distance	30 / 42.5 / 55 / 67.5 / 80 µm	40 / 52.5 / 65 / 77.5 / 90 µm

In connection with the experiments, the resulting optimal parameters were used to build demonstrator parts, a bushing and a part with different types cooling structures, to demonstrate the ability to produce industrial relevant parts and features.

2.4. Methods for analysis

After processing, the specimens were removed from the support structures on the building platform, embed and ground for preparation of the further analysis. For the microscopic analysis of the density the microscope Olympus BX60 (Olympus Europa SE & Co. KG) with a magnification of x5 was utilized. The images were taken in black and white. This way, the ratio between white (dense material) and black pixels (pores) could be evaluated to calculate the relative density.

In addition to the microscopic analysis, the specimens built in the second experimental run were subjected to a hardness test using the INNOVATEST NEXUS 4000 (INNOVATEST Europe BV, Maastricht, The Netherlands). The Vickers hardness was measured with an indentation force of 0.1 N. Every specimen was tested three times to calculate the mean value.

The values of the relative density as well as the hardness values were entered into the DoE table in JMP. For the following statistical analysis, a significance level of 0.05 was implemented. All terms that had no significant influence were removed from to model to achieve a better prognosis quality. To find the optimal parameter combination, the desirability function was used, a mathematical method to find the optimum for the given factors and responses. For example, a relative density of 100 % is the optimum. Consequently, a higher density means a higher desirability.

Furthermore, the parameter estimates, more precisely the estimated model coefficients, were evaluated to assess the strength and direction of the influences of the different parameters on the process result as well as the interactions between them. In this frame, the standard error, the t-ratio (ratio between the esti-

mate and the standard error) and the p-value (for the test that the true parameter is zero) for each of the estimated parameters were also calculated.

3. Results and Discussion

3.1. Experimental runs with cubic specimens

All cubic specimens were built successfully without overbuilding effects or visible defects. Fig. 3 shows the specimens and support structures built onto the platform and one of the built cubes as an example after removal from the building platform.

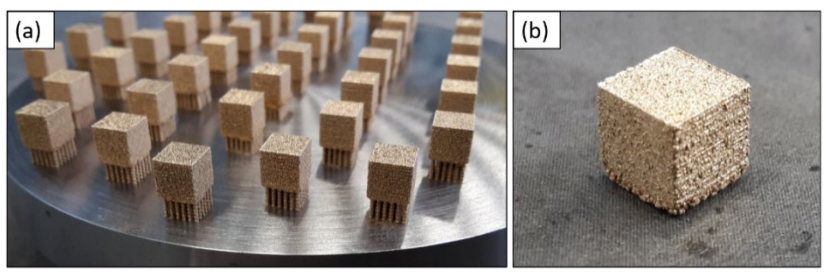

Fig. 3. Cubic specimens: (a) with support structures on building platform; (b) after removal from platform

In the first experimental run, the lowest relative density was 85.1 % (LP=100 W; SS=1400 mm/s; HD=30 µm) and the highest relative density was 99.99 % (LP=200 W; SS=800 mm/s; HD=67.5 µm), both microscopic images shown in Fig. 4. The high porosity resulted from a too low energy input and therefore insufficient melting.

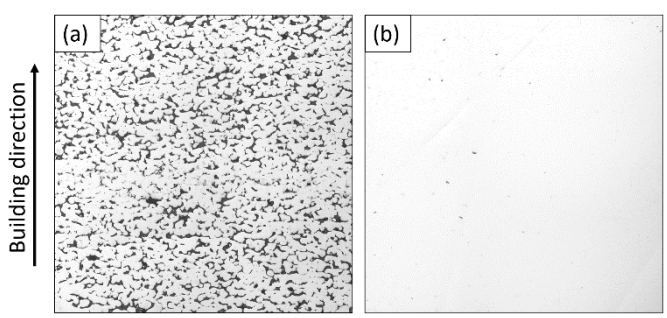

Fig. 4. Microscopic images of first experimental run: (a) relative density of 85.1%; (b) relative density of 99.99 %

Figure 5 shows the prediction profiles of the examined processing parameters determined through regression analysis and the overall desirability. Therein, the calculated 95 % confidence intervals are marked by the grey areas around the graphs. The desirability function was maximized to find the optimal combination of parameter settings (red lines and figures). According to the displayed graphs, the best results (highest desirability) are achievable at a laser power of 192.66 W, a scanning speed of 600 mm/s and a hatch distance of 68.3 µm.

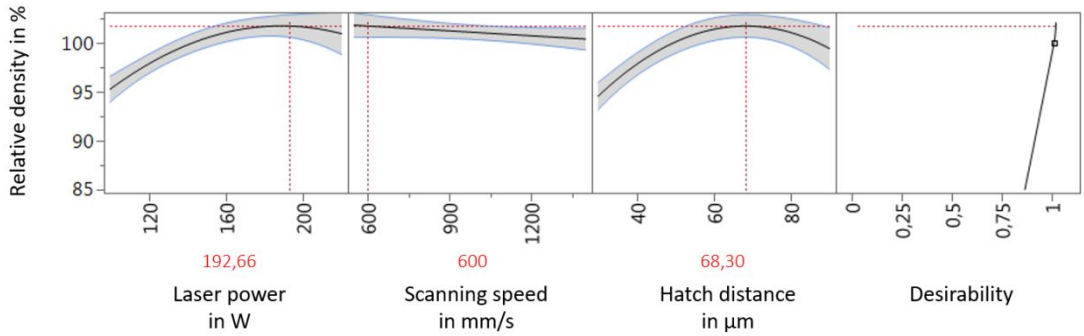

Fig. 5. Prediction profile and desirability of first experimental run

Thereby, the laser power had the strongest influence on the resulting density within the considered limits, followed by the influence of the hatch distance. A positive sign indicates that with increasing parameter value the response value (relative density) also increases. With a negative sign in front of the estimate, the response value decreases for an increasing parameter value. All significant parameter estimates are listed in Fig. 6. As it can also be seen in the graphs of Fig. 5, for the laser power and the hatch distance there is not only a linear influence but also a quadratic correlation between the respective parameter and the relative density.

Term	Estimate	Std Error	t Ratio	Prob>|t|
Intercept	98,406969	0,374559	262,73	<,0001*
laser power [W](100,200)	4,5723151	0,25927	17,64	<,0001*
scanning speed [mm/s](600,1400)	-1,234503	0,25927	-4,76	<,0001*
hatch distance [µm](30,80)	2,1118606	0,25927	8,15	<,0001*
laser power [W]*laser power [W]	-2,05911	0,514263	-4,00	0,0003*
laser power [W]*scanning speed [mm/s]	1,3821513	0,338307	4,09	0,0002*
scanning speed [mm/s]*hatch distance [µm]	-1,148618	0,338307	-3,40	0,0017*
hatch distance [µm]*hatch distance [µm]	-3,06911	0,514263	-5,97	<,0001*

Fig. 6. Significant parameter effects of first experimental run (significance level of 0.05)

Besides the parameter effects, the interactions between the processing parameters are another important point to take into account. Therefore, Fig. 7 shows how the density behaves dependent on the respective parameter when another parameter is fixed. As it can be seen in the graphs and in Fig. 6, there are significant interaction effects between the laser power and the scanning speed and between the scanning speed and the hatch distance. Between the laser power and the hatch distance no significant interaction effect could be detected, hence the lines of the respective graphs are greyed out. That means, that independent of the hatch distance set the influence of the laser power on the relative density is the same.

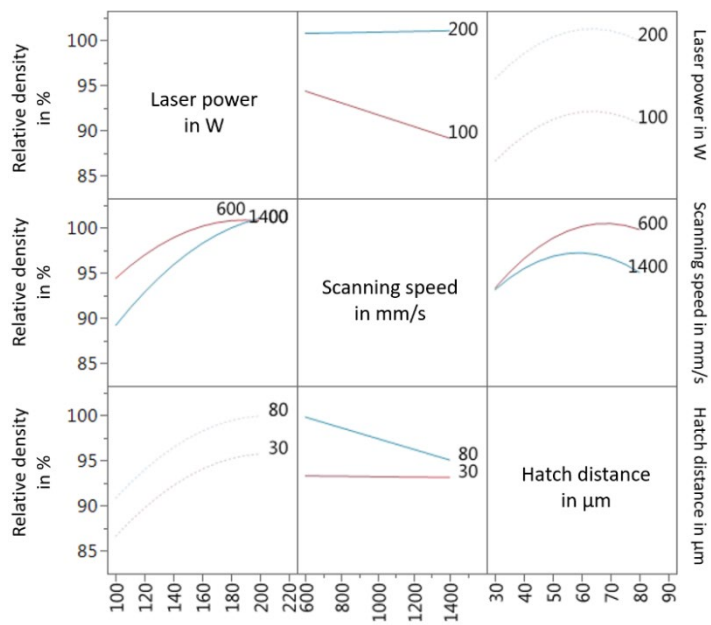

Fig. 7. Interactions between the processing parameters

The influence of the scanning speed is stronger at lower laser power and greater hatch distance. Generally there are higher densities at smaller scanning speeds. At a higher scanning speed, the laser power has a greater influence on the density while at low scanning speeds the influence of the hatch distance is bigger.

Based on the described results of the first experimental run, the parameter settings for the second run were chosen. Greater laser power and hatch distance were implemented, the values for the scanning speed remained the same.

For the relative density, a minimum of 94.7 % (LP=140 W; SS=1400 mm/s; HD=90 µm) and a maximum of 100 % (LP=200 and 220 W; SS=600 and 1400 mm/s; HD=77.5 µm) was reached, the microscopic images are shown in the figure below. In this experimental run, only the cubic effect of the laser power was significant and the desirability was maximum at the highest laser power. The scanning speed and the hatch distance had no significant effect on the relative density. Therefore, the prediction profiles for these parameters are greyed out in Fig. 9.

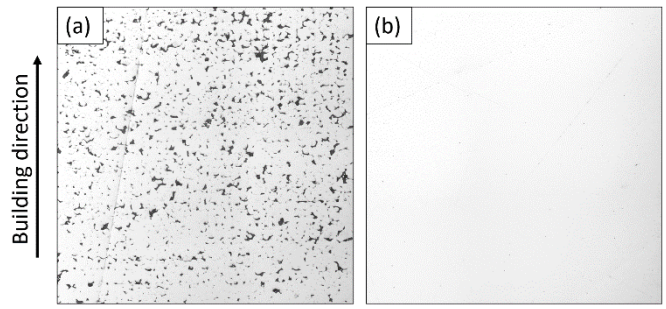

Fig. 8. Microscopic images of second experimental run: (a) relative density of 94.7 %; (b) relative density of 100 %

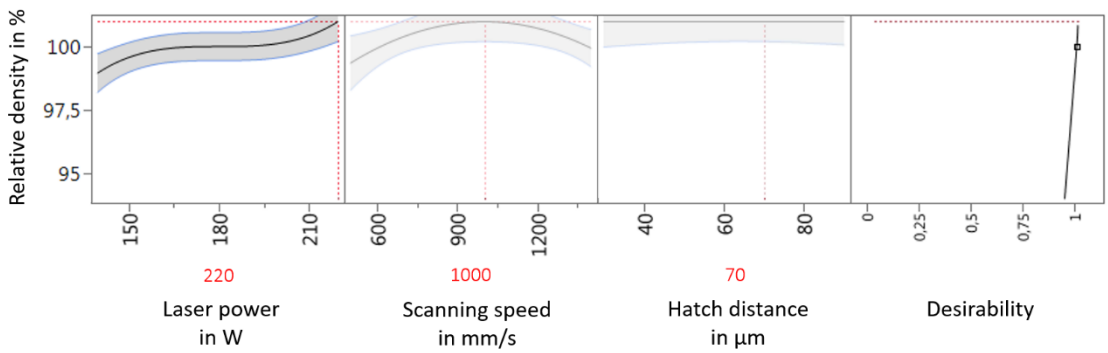

Fig. 9. Prediction profile and desirability of second experimental run

Due to the fact, that there are no other significant effects or interactions between the processing parameters in the second experimental run, no interaction graphs could be generated.

In addition to the microscopic analysis, the specimens built in the second experimental run were also subjected to a hardness test. A maximum hardness value of 211.33 HV (LP=200 W; SS=1200 mm/s; HD=90 µm) and a minimum hardness value of 162.33 HV (LP=160 W; SS=800 mm/s; HD=40 µm) occurred. The overall mean value was 182.3 HV. Generally, the statistical analysis showed no significant influence or interactions of any of the processing parameters on the resulting hardness.

3.2. Demonstrator parts

Based on the findings of the two experimental runs with cubic specimens, a bushing and a part with different cooling structures were manufactured to demonstrate the producibility. Fig. 10 shows the built and post processed parts. The post process consisted of sandblasting and partial grinding to improve the surface quality and to remove the support structures. Considering the values for a maximum relative density and a maximum process efficiency, the following parameter settings were chosen:

- Laser power: 210 W
- Scanning speed: 1000 mm/s
- Hatch distance: 70 µm

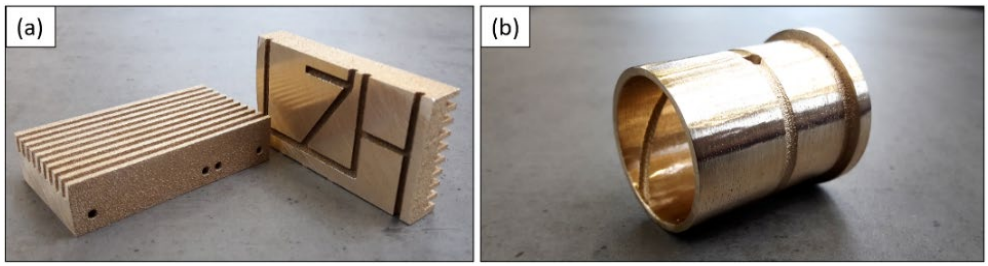

Fig. 10. Demonstrator parts: (a) different cooling structures; (b) bushing

The parts were manufactured successfully without visible defects. Thus, cooling channels with a diameter of 2 mm and cooling fins with a width of 1.4 mm can be built without problems with the found parameter settings.

4. Conclusion

In this work, a set of optimal parameters for the processing of CuSn10 powder via LPBF on the Orlas Creator plant were determined successfully. For the first time, cubic specimens were built based on Design of Experiments and the parameter effects and interactions were evaluated. The laser power had the greatest influence on the relative density and strong interaction effects were detected between laser power and scanning speed and between scanning speed and hatch distance. This indicates that interactions between parameters are an important fact to take into account in further investigations.

The hardness tests did not reveal any significant influences or interaction effects of the processing parameters, presumably, because the examined field of parameter values was too small.

A maximum relative density of 100 % could be achieved and the feasibility of processing different cooling structures and industrial relevant parts could be demonstrated.

Further investigations regarding additional mechanical tests and microstructural analysis as well as the processing of lattice structures and thin walls are planned.

References

Barik, R.C., Wharton, J.A., Wood, R.J.K., Tan, K.S., Stokes, K.R, 2005. Erosion and erosion–corrosion performance of cast and thermally sprayed nickel–aluminium bronze. Wear 259, p. 230-242.

Becker, D., Meiners, W., Wissenbach, K., 2009. Additive manufacturing of copper a alloy by Selective Laser Melting, in: "Lasers in Manufacturing 2009: Proceedings of the Fifth International WLT-Conference Lasers in Manufacturing" Ostendorf, A.,Graf, T., Petring, D., Otto, A., Editors. T-Fachverlag GmbH, Stuttgart, p. 195-200.

Becker, D., 2010. Additive Manufacturing of Parts Made of Copper Alloys Using High Laser Power, International Laser Technology Congress AKL´10.

Frigola, P., Agustsson, R., Boucher, S., Murokh, A., Rosenzweig, J., Travish, G., Faillace, L., Cormier, D., 2008. A Novel Fabrication Technique for the Production of RF Photoinjectors, Proceedings of EPAC08, Genoa, Italy, p. 751-753.

Frigola, P., Harrysson, O. A., Horn, T. J., Aman, R. L., Rigsbee, J. M., Ramirez, D. A., Murr, L. E., Medina, F., Wicker, R. B., Rodriguez, E., 2014. Fabricating Copper Components with Electron Beam Melting, Advanced Materials & Processes, p. 20-24.

Jia, Q., Gu, D., 2014. Selective laser melting additive manufacturing of Inconel 718 superalloy parts: Densification, microstructure and properties. Journal of Alloys and Compounds 585, p. 713-721.

Liu, Z.H., Zhang, D.Q., Sing, S.L., Chua, C.K., Loh, L.E., 2014. Interfacial characterization of SLM parts in multi-material processing: Metallurgical diffusion between 316L stainless steel and C18400 copper alloy. Materials Characterization 94, p. 116-125.

Mao, Z., Zhang, D. Z., Wei, P., Zhang, K., 2017. Manufacturing Feasibility and Forming Properties of Cu-4Sn in Selective Laser Melting. Materials 333, p. 1-12.

Meiners, W., 2011. Fabrication Selective Laser Melting – Additive Manufacturing for series production of the future, Proceedings of INTERMAT Conference.

Ramirez, D. A., Murr, L. E., Li, S. J., Tian, Y. X., Martinez, E., Martinez, J. L., Machado, B. I., Gaytan, S. M., Medina, F., Wicker, R. B., 2011. Open-Cellular Copper Structures Fabricated by Additive Manufacturing Using Electron Beam Melting, Material Science and Engineering: A 528, p. 5379-5386.

Ramirez, D. A., Murr, L. E., Martinez, E., Hernandez, D. H., Martinez, J. L., Machado, B. I., Medina, F., Frigola, P., Wicker, R. B., 2011. Novel Precipitate-Microstructural Architecture Developed in the Fabrication of Solid Copper Components by Additive Manufacturing Using Electron Beam Melting, Acta Materialia 59, p. 4088-4099.

Scudino, S., Unterdörfer, C., Prashanth, K. G., Attar, H., Ellendt, N., Uhlenwinkel, V., Eckert, J., 2015. Additive manufacturing of Cu-10Sn bronze. Materials Letters 156, p. 202-204.

Sun, Z., Tan, X., Tor, S. B., & Yeong, W. Y. (2016).Selective laser melting of stainless steel 316L with lowporosity and high build rates. Materials and Design 104, p. 197-204.

Zhang, L.-C., Attar, H., 2015. Selective Laser Melting of Titanium Alloys and Titanium Matrix Composites for Biomedical Applications: A Review. Advanced Engineering Materials 18, p. 463-475.

Zhang, S., Zhu, H., Hu, Z., Zeng, X., Zhong, F., 2019. Selective Laser Melting of Cu-10Zn alloy powder using high laser power. Powder Technology 342, p. 613-620.